IOP Conf. Series: Materials Science and Engineering **398** (2018) 012033 doi:10.1088/1757-899X/398/1/012033

Synthesis and Characterizations of Nickel (II) Oxide Sub-Micro Rods via co-precipitation Methods

Hui Hui Lim[1], Bahman Amini Horri[1,2] and Babak Salamatinia[1,a]

[1]Discipline of Chemical Engineering, School of Engineering, Monash University Malaysia, Jalan Lagoon Selatan, Malaysia
[2]Department of Chemical Engineering, Faculty of Engineering, University of Surrey, Guildford GU2 7XH, United Kingdom

babak.salamatinia@monash.edu

Abstract. Co-precipitation method has been used for the synthesis of single crystalline Nickel (II) Oxide sub-micro rods. A two-step method was used to synthesise NiO sub-micro rods, in which the first step was the co-precipitation process Nickel (II) Nitrate with Ammonium Oxalate to form Nickel (II) Oxalate (NiC_2O_4), which is the precursor for the precipitates. The precipitate precursor then underwent the calcination process to form NiO sub-micro rods. Synthesized materials undergo Field Emission Scanning Electron Microscope (FESEM), particle size measurement via Zetasizer, elemental analysis via Energy-Dispersive X-ray Spectroscopy (EDX), Fourier Transform Infrared Spectroscopy (FT-IR) and Thermogravimetric Analysis (TGA). The morphology of NiO is found to have uniform rod-like crystals with mean z-diameter between 1600 nm to 2600 nm using Zetasizer.

1. Introduction

Nickel (II) oxide (NiO) is an important p-type semiconductor that exists in cubic lattice structures [1]. NiO particles are suitable materials in many applications, such as lithium battery, fuel cell, supercapacitor, photoelectrodes, gas sensor, chemical catalyst, and electrochromic film [2]. This is mainly because NiO exhibits excellent electrochemical performance, optical electronic performance, photoelectric catalytic, magnetic, thermal, mechanical, and chemical properties [3]. Various quasi-one-dimensional (wires, rods, ribbons) of NiO have attracted significant interest in the past years due to their ability to combine several essential diagnostics, imaging, delivery, and dosage properties, and can still be functionalised. These materials offer considerably higher surface areas than the bulk materials as well as able to function as both structural and functional components in devices [4]. Due to the many advantages of the NiO morphology, many unique synthesis methods have been developed over the years.

NiO nanowires, with a diameter range of 16 to 50 nm, have been synthesised on alumina substrate using the vapor-liquid-solid (VLS) technique with gold particles as the catalyst [5]. In addition, similar NiO nanowires can also be synthesised via hydroxylation and dehydration of nickel foil [6]. In this method, NiO particles are synthesised by soaking nickel foils in a lithium hydroxide solution for a day at room temperature before annealing the foils at high temperature. Mesoporous NiO nanowires were synthesised via hydrothermal treatment of nickel chloride with ethylene glycol at 400 ℃ [7].These mesoporous NiO nanowires have high specific surface areas and high specific capacitance, which become a high lithium storage capacity in lithium-ion cells.

Other than NiO wires, other methods to produce NiO rods have also been developed. NiO nanorods were successfully synthesised using the microwave–assisted method, which was similar to this method. Microwave heating was used with nickel (II) acetate solution to form nickel (II) hydroxide that acted as the precipitate precursor to form NiO [8]. In another study, the microwave-assisted method was used to synthesise polycrystalline NiO nanorods from CH3COO–Ni–OC2H4OH as precipitated precursors [9]. Meanwhile, polycrystalline and single crystalline rod-shaped NiO have synthesised via thermal dehydration of nickel (II) hydroxide that acted as the precipitated precursor [10].
In comparison with other synthesis method, co-precipitation method is a reliable method as the synthesised oxide powders were well-defined and less-agglomerated [11]. Co-precipitation method is believed to be a simple and well-establish method for large-scale synthesis. Various metal oxide particles have been successfully synthesised using the co-precipitation method, such as iron oxide [12], nickel oxide [13], nickel ferrite [14], zinc oxide [15] and tin oxide [16]. Hence, the aim of this research was to synthesise a NiO sub-micro rods via co-precipitation method and to characterise the physiochemical properties of the particles. Particles morphology (FE SEM), particles size measurement (Zetasizer), elemental analysis (EDX), thermal analysis (TGA) and structural analysis (FT-IR) of NiO sub-micro rods were applied to evaluate the performance of the synthesised particles.

2. Materials and methods

All chemicals used in this study were of analytical grade and were used without any modification, unless explained in the methodology. All chemicals are clearly described in Table 1.

Table 1. List of chemicals

Materials	Chemical Formula	Assay
Nickel (II) Nitrate	$Ni(NO_3)_2.6H_2O$	99.999 % trace metal basis
Ammonium Oxalate Monohydrate	$(NH_4)2C_2O_4.H_2O$	≥ 99 %
Ethylene Glycol	$C_2H_6O_2$	≤ 100 %

A two-step method was used to synthesise NiO sub-micro rods, in which the first step was the co-precipitation process of nickel (II) salt with basic oxalate salt to form NiC2O4, which is the precursor for the precipitates. The precipitate precursor then underwent the second steps, which was the calcination process, to form NiO sub-micro rods.
In the co-precipitation step, 12 g/L concentration of nickel (II) salt and 8 g/L concentration of oxalate salt were prepared. Meanwhile, ethylene glycol, as the co-solvent, was used at approximately 40 % of the total amount of reactants in this co-precipitation process. The oxalate salt was stirred and heated up in a beaker (reactor) until the set temperature was reached. Once the desired temperature was reached, the nickel (II) salt was poured into the oxalate salt solution and the timer was started. When the reaction time ended, all the contents of the reactor were immediately poured into centrifuge tubes to centrifuge out the precipitates to prevent further reactions. Once the precipitates have been separated, they were washed with distilled water for three times (pouring distilled water and centrifuging) to ensure that the precipitates were free of co-solvents and unreacted reactants. Each centrifuging step took 10 min or more at 4,500 rpm. The washed precipitates were then dried in the oven at 50 ^{o}C for 24 h.
Then, the dried precipitates were ready for calcination, which was the second step for the synthesis of NiO. The calcination process was fixed at 400 ^{o}C for 8 h, with a ramping rate, R of 2 ^{o}C/min. The calcination process was conducted in a tubular furnace, which was consistently pumped with air to ensure that excess oxygen was available for the calcination reaction. Characterisation tests were performed on the dried precipitates, before and after calcination, for comparison. The characterisation

tests performed in this study were FESEM, TGA, FT-IR, XRD, Zetasizer, ImageJ, and Raman Spectroscopy.

3. Results and discussions

Table 2 lists the co-precipitated NiO sub-micro rods that were obtained at various co-precipitation temperatures and dwelling times. Table 2 also lists the mean size of the sub-micro rods in terms of the mean major axis (length of rod), minor axis (rod diameter), and aspect ratio. The mean size of these sub-micro rods were obtained using ImageJ software from a group of randomly selected samples, with a sample size of 25.

Table 2. Dimensions of NiO sub-micro rods obtained from various co-precipitation temperatures and dwelling times

Sample	Mean Major Axis (μm)	Mean Minor Axis (μm)	Mean Aspect Ratio, AR
NiO50 ºC(60 min)	0.883	0.245	3.883
NiO75 ºC(30 min)	1.677	0.465	3.738
NiO75 ºC(60 min)	2.413	1.077	2.277
NiO100 ºC(6 min)	1.346	0.254	5.296
NiO100 ºC(7 min)	1.723	0.392	4.724
NiO100 ºC(8 min)	1.615	0.432	4.014
NiO100 ºC(9 min)	1.882	0.444	4.433
NiO100 ºC(10 min)	1.514	0.424	3.788
NiO100 ºC(30 min)	3.199	1.243	2.605
NiO100 ºC(60 min)	3.946	1.852	2.187

3.1 Morphology (FE SEM)

3.1.1 Effect of co-precipitation temperature. Figure 1. shows FESEM images of NiO synthesised at different temperatures: (a) 50 ℃, (b) 75 ℃, and (c) 100 ℃ at a constant dwelling time at 60 min. It was found that the resulting NiO particles were in the form of smooth, cylindrical rod-like crystals. Under higher magnification, a rough structure was observed on the surface of the rod, which could be the outcome of the degradation of organic groups and phase transformation [9].

These NiO rods underwent two stages, which were the nucleation stage of atom formed by metal salt reduction and the crystal growth stage from nuclei through atomic growth [17]. When results from various temperatures at constant reaction time were compared, it was observed that the size of the NiO sub-micro rods had increased with increasing temperature. This can be observed from the increasing mean major axis (0.883 μm, 2.413 μm and 3.946 μm), and mean minor axis (0.245 μm, 1.077 μm and 1.852 μm), as tabulated in Table 2. However, the mean aspect ratio, AR had decreased to 3.883, 2.277 and 2.187 when the co-precipitation temperature was increased. The decreasing trend of AR was because crystals tend to elongate along the c-axis in the crystal lattice when the particles size increases [18].

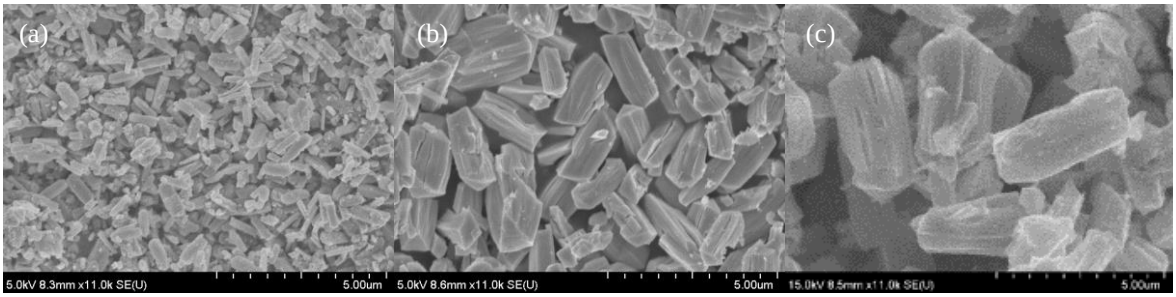

Figure 1. FESEM images of samples: (a) NiO 50 ℃(60 min), (b) NiO 75 ℃(60 min), and (c) NiO 100 ℃(60 min) at constant co-precipitation dwelling time of 60 min

3.1.2 *Effect of co-precipitation dwelling time.* Figure 2 shows the comparison between FESEM images of NiO sub-micro rods synthesised at a constant 100 ℃, with different co-precipitation dwelling times. Figure 2 (a) shows the FESEM images of NiO sub-micro rods synthesised at the shortest time, which was at 6 min. No precipitate had formed for dwelling time of shorter than 6 min as no nuclei was formed at the beginning of the co-precipitation reaction, even when the saturation of metal atom concentration was achieved. Crystals growth stage would only start when metal atom concentration had decreased lower than the nucleation concentration [17].

At 6 min, the NiO sub-micro rods have the highest aspect ratio of 5.296 with the smallest mean minor axis at 0.254 μm. Figure 2 (b), Figure 2 (c), Figure 2 (d), and Figure 2 (e) show FESEM images of NiO sub-micro rods synthesised at 7 min, 8 min, 9 min, and 10 min of dwelling time, respectively. These NiO sub-micro rods had shown increments in mean minor axis values (0.392 μm, 0.432 μm, 0.444 μm, and 0.424 μm, respectively), and a decreasing trend of mean aspect ratio values (4.724, 4.014, 4.433, and 3.788, respectively). Additionally, these NiO sub-micro rods had more uniform particles compared to the rods formed at only 6 min of dwelling time.
Figure 2 (f) and Figure 2 (g) show FESEM images of NiO sub-micro rods after longer dwelling times of 30 min and 60 min. The mean minor axis of the NiO sub-micro rods had significantly increased to 1.243 μm and 1.852 μm, respectively with these times. When the dwelling time was increased, more nuclei that were formed during nucleation could reach the crystal growth stage. During this stage, atoms or molecules in the solution will be integrated into the surface of the crystals, contributing to the increase in crystal size [19]. Hence, the size of the NiO sub-micro could increase as the dwelling time increases.

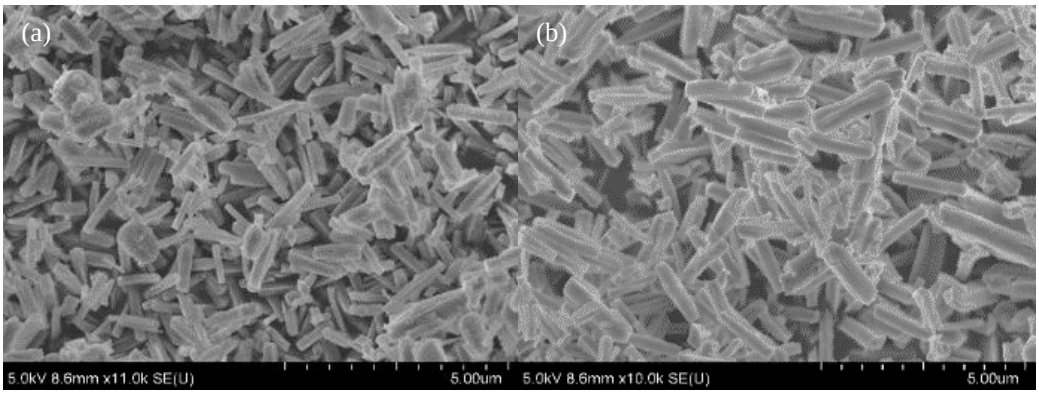

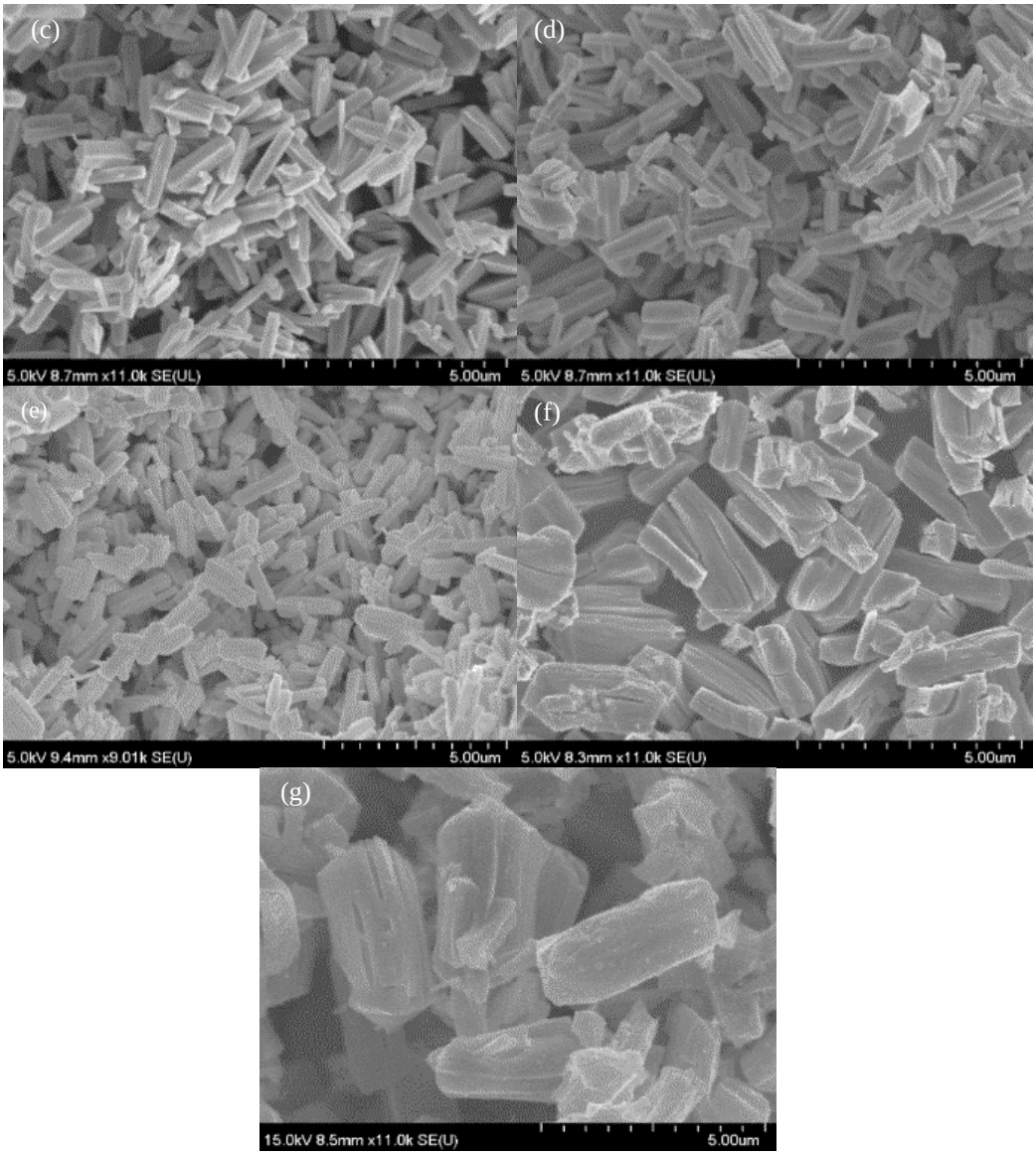

Figure 2. FESEM images of: (a) NiO100(6), (b) NiO100(7), (c) NiO100(8), (d) NiO100(9), (e) NiO100(10), (f) NiO100(30), and (g) NiO100(60) at constant co-precipitation temperature of 100 ℃

3.2 Particle size measurement

Figure 3 shows the particles size distribution for various co-precipitation durations at 100 ℃, as obtained from the Zetasizer. The particles size distributions for all reaction times were symmetrical bell-shaped curves, which were similar to a normal distribution curve [20]. The particles size distribution has justified that by increasing the reaction time, the size of the NiO sub-micro rods would concurrently increase. Hence, the mean z-diameter was found to be at 1623 nm, 2083 nm, and 2639 nm, with respective to the increased time. From the particle size distribution, it was found that a longer reaction time would give a narrower size range, causing the distribution curve to have a sharper peak. NiO sub-micro rods, which resulted after 60 min of reaction time, had the smallest size range from 1990 – 3580 nm, followed by the rods after 30 min (1484 – 3091 nm), and 10 min (825 – 3580 nm). These results showed that a longer reaction time would give more uniformly sized NiO sub-micro rods.

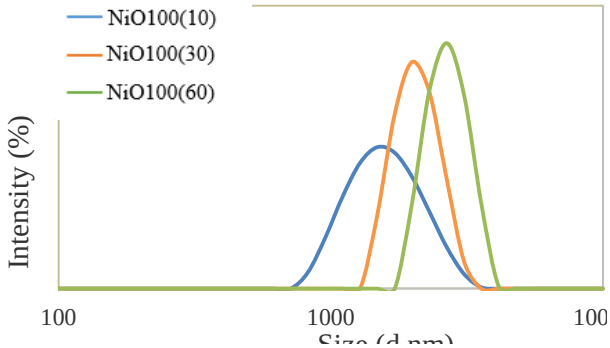

Figure 3. Intensity of particle size distribution of NiO sub-micro rods at different reaction dwelling times

3.3 Elemental analysis (XRD)

Elemental analysis was conducted by scanning FESEM images using an EDX to obtain the elemental composition of the synthesised material. NiC_2O_4 and NiO that were synthesised at a reaction temperature of 100 ˚C for 10 min were used to conduct the elemental analysis. EDX reported that NiC_2O_4 was made up of mainly oxygen with 58.93 atomic %, 21.64 atomic % of carbon, and 19.43 atomic % of nickel. Using the chemical formula for NiC_2O_4, the theoretical atomic % was determined to be 57.14 %, 28.57 %, and 14.29 % for oxygen, carbon, and nickel, respectively, which showed similar trends with the EDX results.

Since NiO was made up of 1:1 atomic ratio of nickel to oxygen, the theoretical atomic % for nickel and oxygen was 50 %. EDX reported similar results for the synthesised NiO, which consisted of 47.78 atomic % of nickel and 52.22 atomic % of oxygen. The EDX results had also shown that the calcination reaction had caused the NiC_2O_4 to decompose into high purity NiO, with no side reaction that could have produced by-products like nickel or nickel carbonate [21]. This can be further justified by conducting the FT-IR and thermal analyses.

3.4 FT-IR

Figure 4 shows the FT-IR spectra of NiC2O4 and NiO synthesised at 100 ˚C for 10 min. The FT-IR spectra of NiC2O4 exhibited a weak, broad band at 3390 cm-1 that corresponded with the O-H stretching vibration, and a strong broad band at 1600 cm-1 that correlated to the H-O-H bending vibration of water [22]. Another two sharp peaks were observed at wavenumber 1360 cm-1 and 1310 cm-1, which indicated the C-O vibration in the CO32- group and the C-O stretching of oxalate ion, respectively [21].

Meanwhile, the FT-IR spectra of NiO showed one peak at 550 cm-1 that can be attributed to the Ni-O bond stretching vibration [23]. No NiC2O4 characteristic bonds had appeared in the NiO spectra, indicating that all NiC2O4 had decomposed into NiO during calcination. Hence, the synthesised NiO was of high purity, with no traces of impurities.

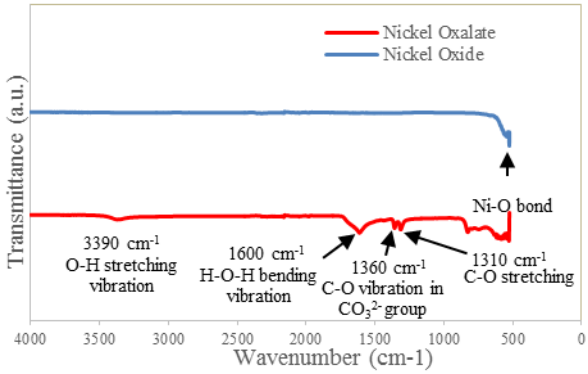

Figure 4. FT-IR Spectra of NiC2O4 and NiO

3.5 Thermal analysis (TGA)

TGA curve of NiC_2O_4 and NiO in air at a heating rate of 10 ˚C/min are shown in Figure 5. TGA curves of NiC_2O_4 clearly showed two well-defined steps, indicating the dehydration and decomposition of NiC_2O_4 upon heating. The first significant weight loss of 17.4 % occurred between 180 ˚C and 235 ˚C, which could attributed to the dehydration process of NiC_2O_4 dehydrate to anhydrous oxalate [24]. This step showed an endothermic characteristic with a DTA peak at 225 ˚C.
On the other hand, the second step weight loss occurred between 315 to 340 ˚C, which showed an exothermic DTA peak at 330 ˚C. The weight loss of 34.9 % during the second step could be attributed to the decomposition of anhydrous oxalate to NiO [24]. Hence, a minimum calcination temperature of 340 ˚C was applied to form NiO from NiC_2O_4 dihydrate. TGA curve of NiO showed no/minimal changes in weight loss, which indicated that the synthesised NiO was thermally stable and did not experience change in state upon extreme heating.

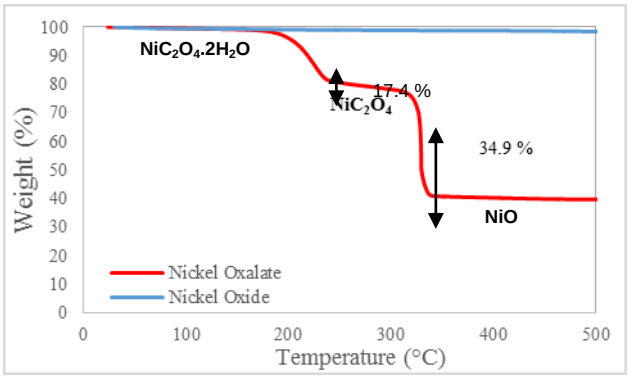

Figure 5. TGA curve of NiC2O4 and NiO in air Conclusion

High purity NiO sub-micro rods have been successfully synthesised using the co-precipitation method. The surface morphology of NiO showed it to be in the form of rod-shaped single crystals, with crystal size that depended on the co-precipitation time and temperature. FESEM images showed that the crystal size had increased with increasing co-precipitation temperature and dwelling time. When the co-precipitation temperature was increased from 50 to 75 oC and 100 oC at a constant dwelling time of 60 min. On the other hand, increasing the dwelling time at 100 oC had led to increasing rod diameter. These results were further proven using zetasising which showed increases in the mean z-diameter of the particles with increasing co-precipition dwelling time. EDX found that the atomic percentages of both oxalate and oxide had tallies with the theoretical atomic percentages. Furthermore, FT-IR was conducted to identify the chemical bonding of the elements. The NiC2O4 sample had peaks at 3390 cm-1 (O-H stretching vibration), 1600 cm-1 (H-O-H bending vibration), 1360 cm-1 (C-O vibration), and 1310 cm-1 (C-O stretching). However, these peaks were not found in the NiO

sample and only one peak was found at 550 cm-1 showing no traces of impurities. Lastly, the TGA result of NiC2O4 showed two well-defined steps indicating the dehydration and decomposition of NiC2O4. In the meantime, the TGA result of NiO showed minimal changes in weight loss, thus indicating a thermally stable NiO.

4. References

[1] M. Tadic, D. Nikolic, M. Panjan, and G. R. Blake, Magnetic properties of NiO (nickel oxide) nanoparticles: Blocking temperature and Neel temperature, Journal of Alloys and Compounds, 647, pp. 1061-1068 (2015).

[2] M. El-Kemary, N. Nagy, and I. El-Mehasseb, Nickel oxide nanoparticles: Synthesis and spectral studies of interactions with glucose, Materials Science in Semiconductor Processing, 16, 6, pp. 1747-1752 (2013).

[3] M. M. Ba-Abbad, P. V. Chai, M. S. Takriff, A. Benamor, and A. W. Mohammad, Optimization of nickel oxide nanoparticle synthesis through the sol–gel method using Box–Behnken design, Materials & Design, 86, pp. 948-956 (2015).

[4] T. Ahmad, A. Ganguly, J. Ahmed, A. K. Ganguli, and O. A. A. Alhartomy, Nanorods of transition metal oxalates: A versatile route to the oxide nanoparticles, Arabian Journal of Chemistry, 4, 2, pp. 125-134 (2011).

[5] N. Kaur, E. Comini, N. Poli, D. Zappa, and G. Sberveglieri, Nickel Oxide Nanowires Growth by VLS techniqu for gas sensing application, Procedia Engineering, 120, pp. 760-763 (2015).

[6] K. Sekiya, K. Nagato, T. Hamaguchi, and M. Nakao, Morphology control of nickel oxide nanowires, Microelectronic Engineering, 98, pp. 532-535 (2012).

[7] D. Su, H.-S. Kim, W.-S. Kim, and G. Wang, Mesoporous Nickel Oxide Nanowires: Hydrothermal Synthesis, Characterisation and Applications for Lithium-Ion Batteries and Supercapacitors with Superior Performance, Chemistry – A European Journal, 18, 26, pp. 8224-8229 (2012).

[8] M. A. Bhosale and B. M. Bhanage, Rapid synthesis of nickel oxide nanorods and its applications in catalysis, Advanced Powder Technology, 26, 2, pp. 422-427 (2015).

[9] X. Song and L. Gao, Facile Synthesis of Polycrystalline NiO Nanorods Assisted by Microwave Heating, Journal of the American Ceramic Society, 91, 10, pp. 3465-3468 (2008).

[10] N. Srivastava and P. C. Srivastava, Synthesis and characterization of (single- and poly-) crystalline NiO nanorods by a simple chemical route, Physica E: Low-dimensional Systems and Nanostructures, 42, 9, pp. 2225-2230 (2010).

[11] Z. Shao, W. Zhou, and Z. Zhu, Advanced synthesis of materials for intermediate-temperature solid oxide fuel cells, Progress in Materials Science, 57, 4, pp. 804-874 (2012).

[12] N. D. Kandpal, N. Sah, R. Loshali, R. Joshi, and J. Prasad, Co-precipitation method of synthesis and charactrization of iron oxide nanoparticles, Journal of Scientific & Industrial Research, 73, pp. 87-90 (2014).

[13] R. Kumar, A. Sharma, N. Kishore, and N. Budhiraja, Preparation and Characterization of NiO Nanoparticles Co-Precipitation Method, International Journal of Engineering, Applied and Management Sciences Paradigms, 6, 1 (2013).

[14] K. Velmurugan, V. S. K. Venkatachalapathy, and S. Sendhilnathan, Synthesis of Nickel Zinc Iron Nanoparticles by Coprecipitation Technique, Materials Research pp. 299-303 (2010)

[15] A. J. Ahamed and P. V. Kumar, "Synthesis and characterization of ZnO nanoparticles by co-precipitation method at room temperature, Journal of Chemical and Pharmaceutical Research, 8, 5, pp. 624-628 (2016).

[16] L. I. Nadaf and K. S. Venkatesh, Synthesis and Characterization of Tin Oxide Nanoparticles by Co-precipitation Method, IOSR Journal of Applied Chemistry, 9, 2, pp. 1-4 (2016).

[17] J. Lai, W. Niu, R. Luque, and G. Xu, Solvothermal synthesis of metal nanocrystals and their applications, Nano Today, 10, 2, pp. 240-267 (2015).

[18] R. Ho, D. A. Wilson, and J. Y. Y. Heng, Crystal Habits and the Variation in Surface Energy Heterogeneity, Crystal Growth & Design, 9, 11, pp. 4907-4911 (2009).

[19] P. Cubillas and M. W. Anderson, Synthesis Mechanism: Crystal Growth and Nucleation, in Zeolites and Catalysis, Synthesis, Reactios and Applications, 1, J. Cejka, A. Corma, and S. Zones, Eds. Weinheim: Wiley-VCH Verlag GmbH & Co. KGaA (2010)
[20] E.Weisstein. (2016). Normal Distribution. Available: http://mathworld.wolfram.com/NormalDistribution.html
[21] B. Małecka, A. Małecki, E. Drożdż-Cieśla, L. Tortet, P. Llewellyn, and F. Rouquerol, Some aspects of thermal decomposition of NiC2O4 2H2O, Thermochimica Acta, 466, 1, pp. 57-62 (2007).
[22] S. V. Ganachari, R. Bhat, R. Deshpande, and V. A, Synthesis and characteization of nickel oxide nanoparticles by self-propagatinglow temperature combustion method, Recent Research in Science and Technology, 4, 4, pp. 50-53 (2012).
[23] A. E.-A. A. Said, M. M. A. El-Wahab, S. A. Soliman, and M. N. Goda, Synthesis and Characterization of Nano CuO-NiO Mixed Oxides, Nanoscience and Nanoengineering, 2, 1, pp. 17-28 (2014).
[24] D. Zhan, C. Cong, K. Diakite, Y. Tao, and K. Zhang, Kinetics of thermal decomposition of nickel oxalate dihydrate in air, Thermochimica Acta, 430, 1, pp. 101-105 (2005).

Acknowledgments
This research was funded by Ministry of Science, Technology and Innovation (MOSTI) Science Fund Project (03-02-10-SF0259). We thank Monash University Malaysia for supported this research by providing an equipped research environment. We would also like to show our gratitude to the laboratories technician/staff in Monash who provide expertise that greatly assisted this research.